# Evidence of Potts-Nematic Superfluidity in a Hexagonal $sp^2$ Optical Lattice

Shengjie Jin,[1] Wenjun Zhang,[1] Xinxin Guo,[1] Xuzong Chen,[1] Xiaoji Zhou,[1,2,*] and Xiaopeng Li[3,4,†]
[1]State Key Laboratory of Advanced Optical Communication System and Network, Department of Electronics, Peking University, Beijing 100871, China
[2]Collaborative Innovation Center of Extreme Optics, Shanxi University, Taiyuan, Shanxi 030006, China
[3]State Key Laboratory of Surface Physics, Institute of Nanoelectronics and Quantum Computing, Department of Physics, Fudan University, Shanghai 200438, China
[4]Shanghai Qizhi Institute, AI Tower, Xuhui District, Shanghai 200232, China

(Received 10 April 2020; revised 29 August 2020; accepted 21 December 2020; published 21 January 2021)

As in between liquid and crystal phases lies a nematic liquid crystal, which breaks rotation with preservation of translation symmetry, there is a nematic superfluid phase bridging a superfluid and a supersolid. The nematic order also emerges in interacting electrons and has been found to largely intertwine with multiorbital correlation in high-temperature superconductivity, where Ising nematicity arises from a four-fold rotation symmetry $C_4$ broken down to $C_2$. Here, we report an observation of a three-state ($\mathbb{Z}_3$) quantum nematic order, dubbed "Potts-nematicity", in a system of cold atoms loaded in an excited band of a hexagonal optical lattice described by an $sp^2$-orbital hybridized model. This Potts-nematic quantum state spontaneously breaks a three-fold rotation symmetry of the lattice, qualitatively distinct from the Ising nematicity. Our field theory analysis shows that the Potts-nematic order is stabilized by intricate renormalization effects enabled by strong interorbital mixing present in the hexagonal lattice. This discovery paves a way to investigate quantum vestigial orders in multiorbital atomic superfluids.

DOI: 10.1103/PhysRevLett.126.035301

In electronic materials, the existence of nematic order [1] has been established in high temperature superconductors such as cuprates [2] and iron-based superconductors [3–6]. The quantum liquid crystal phase is of great importance to the fundamental understanding of high temperature superconductivity. The investigation of intertwined vestigial orders in multiorbital superconductivity that incorporates nematicity has been attracting much attention [6] in recent years. In these superconducting materials, an Ising-nematic order is most predominantly observed, where the nematic orientation has only two choices. In such systems, what drives the nematic order has ambiguity, for it is difficult to separate the electron correlation effects from material structural transitions [4].

The system of ultracold neutral atoms confined in optical lattices has a large degree of controllability. The backaction from atoms to the confining laser potential is typically negligible, making the structural transition avoidable. As an effort to build an optical lattice emulator for multiorbital physics [7,8], excited band condensation of cold atoms has been achieved in one- [9,10] and two-dimensional lattices [11–14]. A crucial difference of such condensates from the ground-state condensate is that the physics is generically described by a multicomponent order parameter that respects crystalline symmetries [7,8], distinctive from single-component [15] or multicomponent spinor condensates [16]. At the level of effective field theory description, this atomic system shares similarity as multiorbital iron-based superconductors and enjoys more controllability. Interaction driven orbital orders such as chiral symmetry breaking [8,11,12,14], and dynamical phase sliding [10] have been reported in multiorbital settings of cold atoms. But many-body correlation effects beyond mean field theory have not been observed so far in such experimental systems.

Here, we report observation of a Potts-nematic quantum state in a system of cold atoms loaded into the second band of a hexagonal optical lattice. The emergence of this novel phase is not captured by a simple mean field theory. First, we prepare an atomic Bose-Einstein condensate (BEC) in the ground band which respects all symmetries of the lattice and, then, project the atomic sample onto the band maximum of the second band using a lattice quench (see Fig. 1). The phase coherence in the state will immediately disappear and, then, reemerge within a few milliseconds. During this process of phase-coherence reformation, the quantum state spontaneously chooses one orientation, giving rise to a three-state Potts nematicity, which is qualitatively distinct from the commonly observed Ising-nematic order in multiorbital superconductors. In the dynamical evolution, the lifetime of the Potts-nematic state is around 20 ms. The emergence and disappearance of the Potts-nematic order in dynamics are found to coincide with the atomic phase coherence in the excited band. Our theory analysis shows that the Potts-nematic symmetry breaking is captured by an orbital-$sp^2$ (with $s$, $p_x$, and $p_y$ hybridized)

 

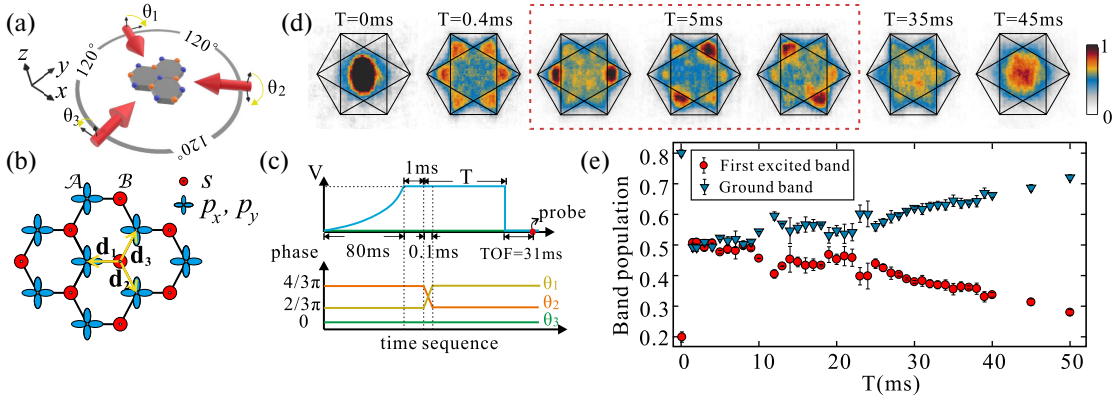


FIG. 1. Experimental protocol of loading atoms into the excited $sp^2$ band of the hexagonal optical lattice. (a) Illustrates the arrangement of the laser beams forming the hexagonal lattice. There are three laser beams in the $x$-$y$ plane with laser-wavelength $\lambda = 1064$ nm forming an optical hexagonal lattice [17]. The three angles $\theta_{1,2,3}$ represent the relative phases of the elliptical polarization of the light. (b) The geometry of the hexagonal lattice, having two sets of sublattices labeled by $\mathcal{A}$ and $\mathcal{B}$. The lattice is formed taking $\{\theta_1, \theta_2, \theta_3\} = \{4\pi/3, 2\pi/3, 0\}$ or $\{2\pi/3, 4\pi/3, 0\}$. (c) The time sequence implemented in the experiment to load atoms from the lowest to the second band. (d) The band-mapping TOF images with $T = 0, 0.4, 5, 35, 45$ ms. When $T = 5$ ms, three different band-mapping TOF corresponding to three nematic orientations are shown in the red dashed box. (e) The measured time evolution of the atomic population in the ground and first-excited bands normalized by their sum. Here, we average over five experimental runs for each data point, with the error bar denoting the statistical error.

lattice model [see Fig. 1(b)] [27–29], yet with strong many-body renormalization effects caused by single-particle interorbital mixing between $p_x$ and $p_y$. This effect is absent in the square lattice [30] but unavoidable in the hexagonal lattice, which makes the $p_x$-$p_y$ orbital Josephson coupling generically renormalize from the positive to the negative side in our field theory analysis. This work opens up a wide window for exploring rich correlated vestigial orders in orbital-mixed atomic superfluids [27–29,31–34].

Our experiment is based on a $^{87}$Rb BEC with $10^5$ atoms in a quasi-2D hexagonal optical lattice, composed of two classes of tube-shaped lattice sites, denoted as $\mathcal{A}$ and $\mathcal{B}$ (see Fig. 1). Atoms are confined in 800 tubes, with each tube containing 60 atoms on average. The temperature of atoms before loading into the optical lattice is 75 nK, for which about 70% of the atoms are condensed in our experiment.

The lattice potential is formed by three intersecting far-red-detuned laser beams in the $x$-$y$ plane with an enclosing angle of 120°. Each beam is formed by combining two linearly polarized lights with polarization directions oriented in the $x$-$y$ plane (denoted as in light) and along the $z$ axis (denoted as out light), respectively. The in and out light form an inversion symmetric honeycomb lattice, and a simple triangular lattice, respectively, whose lattice strengths ($V_{\text{in}}$ and $V_{\text{out}}$) are separately tunable. The out-to-in light intensity ratio is denoted as $\tan^2\alpha = V_{\text{out}}/V_{\text{in}}$. The well depths at $\mathcal{A}$ and $\mathcal{B}$ sites are made different by aligning two lattices in a way that $\mathcal{A}$ ($\mathcal{B}$) sites of the honeycomb lattice are enhanced (weakened) by the potential minima (maxima) of the triangular lattice or the other way around, which is controllable by choosing relative phases between the in and out light, denoted as $\theta_{1,2,3}$ [17].

The lattice has a similar geometry as in previous experiments [35–37]. First, we adiabatically load the BEC into the ground band optical lattice. The phase differences are initially set to be $\theta_{1,2,3} = (2\pi/3, 4\pi/3, 0)$, for which the $\mathcal{B}$ sites are deeper than the $\mathcal{A}$ sites. The ground state BEC forms at the $\Gamma$ point, which respects all lattice symmetries. In real space, atoms mainly reside in the $s$ orbitals of $\mathcal{B}$ sites. Then, we adopt the projection protocol developed for loading atoms to excited bands of a square lattice [11]. We switch the phase differences $\theta_{1,2,3}$ rapidly (within 0.1 ms) to the reverse case with $\theta_{1,2,3} = (4\pi/3, 2\pi/3, 0)$, making $\mathcal{A}$ sites much lower than $\mathcal{B}$. In this way, the atomic sample is directly projected onto the excited band. By selecting an appropriate combination of laser intensities having $V_{\text{in}} + V_{\text{out}} = 30E_R$ ($E_R$ the single-photon recoil energy), and $\alpha = 14°$, a second-band population ratio of 50% is achieved, as measured by band mapping techniques (Fig. 1). In this Letter, we choose laser intensity such that the $s$ orbital of $\mathcal{B}$ sites are near resonance with $p_{x,y}$ orbitals of $\mathcal{A}$ sites in the final lattice, and consequently, the second, third, and fourth bands are close-by in energy [17].

The quantum tunnelings at the final stage are, then, described by an $sp^2$-orbital-hybridized model

$$H_0 = t_{sp}\sum_{\mathbf{r}\in\mathcal{B}}\sum_{a=1,2,3}[\hat{s}^\dagger_{\mathbf{r}}(\vec{\hat{p}}_{\mathbf{r}+\mathbf{d}_a}\cdot\mathbf{e}_a) + \text{H.c.}] - \mu_s\sum_{\mathbf{r}\in\mathcal{B}}\hat{s}^\dagger_{\mathbf{r}}\hat{s}_{\mathbf{r}} - \mu_p\sum_{\mathbf{r}'\in\mathcal{A}}\vec{\hat{p}}^\dagger_{\mathbf{r}'}\cdot\vec{\hat{p}}_{\mathbf{r}'}. \quad (1)$$

Here, $\hat{s}$ and $\hat{p}$ represent quantum mechanical annihilation operators for $s$ and $p$ orbitals, and the shorthand notation $\vec{\hat{p}} = (\hat{p}_x, \hat{p}_y)$. The unit vectors $\mathbf{e}_1 = (-1, 0)$,

$\mathbf{e}_2 = (1/2, -\sqrt{3}/2)$, and $\mathbf{e}_3 = (1/2, \sqrt{3}/2)$ and corresponding $\mathbf{d}_a = (2\lambda/3\sqrt{3})\mathbf{e}_a$ mark the relative position between the two sublattices (Fig. 1), with $\lambda$ the laser wavelength. The quantum tunneling between $\mathcal{A}$ and $\mathcal{B}$ sublattices is $t_{sp}$, which is about $2\pi \times 540$ Hz in our experiment. The chemical potentials for $s$ and $p$ orbitals are denoted as $\mu_s$, and $\mu_p$, respectively. The many-body quantum effects are modeled by the $s$-orbital interaction, $H_{\text{int,s}} = U_s/2 \sum_{\mathbf{r}\in\mathcal{B}} \hat{s}^\dagger_{\mathbf{r}} \hat{s}^\dagger_{\mathbf{r}} \hat{s}_{\mathbf{r}} \hat{s}_{\mathbf{r}}$, and the $p$-orbital interaction

$$H_{\text{int,p}} = \sum_{\mathbf{r}\in\mathcal{A}} \{J[\hat{p}^\dagger_{x,\mathbf{r}} \hat{p}^\dagger_{x,\mathbf{r}} \hat{p}_{y,\mathbf{r}} \hat{p}_{y,\mathbf{r}} + \text{H.c.}]\} + \sum_{\mathbf{r}\in\mathcal{A}} \left\{ \frac{1}{2} \sum_{\alpha,\beta\in\{x,y\}} U_{p,\alpha\beta} \hat{p}^\dagger_{\alpha,\mathbf{r}} \hat{p}^\dagger_{\beta,\mathbf{r}} \hat{p}_{\beta,\mathbf{r}} \hat{p}_{\alpha,\mathbf{r}} \right\}. \quad (2)$$

In the language of group theory, the $s$ orbital transforms according to a one-dimensional representation of the lattice symmetry group $C_{3v}$ ($A_1$), and $p$ orbitals correspond to the two-dimensional representation ($E$). The $p$-orbital couplings are constrained by $U_{p,xx} = U_{p,yy} \equiv U_{p\parallel}$, $U_{p,xy} = U_{p,yx} \equiv U_{p\perp}$, $J = (U_{p\parallel} - U_{p\perp})/2$, according to symmetry analysis. In our experiment, the density interactions $U_s$, $U_{p\parallel}$, and $U_{p\perp}$ are found to be comparable with the tunneling $t_{sp}$, and the Josephson coupling $J$ is 1 order of magnitude smaller [17]. By loading cold atoms into the excited band in our hexagonal lattice, a quantum many-body system with $sp^2$-orbital hybridization is achieved, which is a versatile platform for hosting rich physics such as large-gap topological phases [38,39], exotic orbital frustration [32,33], and novel carbon structure [40] analogies.

Right after the lattice switch, we have cold atoms symmetrically residing on the $\Gamma$ point of the second band. Then, we hold the system for 5 ms and take the measurements of momentum distribution of the system through TOF. We repeat the same experiment 600 times and, then, perform statistics on the independently obtained TOF images. The results are shown in Fig. 2. To diagnose the Potts-nematic order, we divide the momentum space into three regions marked as $\square$, $\bigcirc$, and $\triangle$, related to each other by a $C_3$ rotation [see Fig. 2(a)]. The total population in these three different regions are denoted as $n_\square$, $n_\bigcirc$, and $n_\triangle$, correspondingly. We define a complex valued Potts-nematic contrast (PNC) as

$$\text{PNC} = \frac{n_\square + e^{i2\pi/3} n_\bigcirc + e^{i4\pi/3} n_\triangle}{n_\square + n_\bigcirc + n_\triangle}, \quad (3)$$

which vanishes only when the $C_3$ symmetry is unbroken. When the symmetry is completely broken, PNC takes discrete values from $(1, e^{i2\pi/3}, e^{i4\pi/3})$. The occurrence of PNC collected from consecutive experimental runs [Fig. 2(b)] explicitly shows that the atomic quantum state randomly acquires one of the three orientations. The occurrence probability in the three orientations is approximately equal, with the slight difference caused by experimental imperfection. For example, a gradient magnetic field is added along the gravitational direction to compensate for the Earth's gravity. One of three laser beams (the one along the gravitational direction) forming the hexagonal lattice is linearly polarized while the other two are elliptically polarized. The laser beams then have different degrees of fluctuations. The slight asymmetry observed in the distribution of the Potts-nematic order is attributed to the imperfect equivalence among the three directions. We expect that switching to a lattice perpendicular to the gravitational direction could improve the symmetry of the distribution, which is not carried out here due to technical limitations in our experiment.

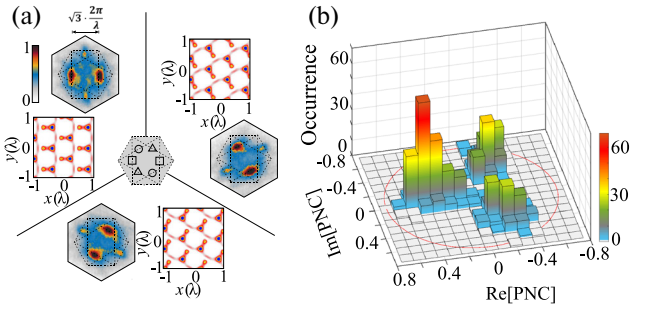


FIG. 2. Spontaneous Potts-nematic symmetry breaking in the hexagonal optical lattice. (a) The averaged momentum distribution. Atoms loaded in the excited band are found to spontaneously accumulate at one of the three $M$ points. We introduce a Potts-nematic contrast [PNC in Eq. (3)], where $n_{\square,\bigcirc,\triangle}$ correspond to momentum distributions in three separate regions as marked in the middle of (a), related to each other by a three-fold lattice rotational symmetry. In the three panels, first, we classify the experimental images into three classes according to the polar angle of the nematic contrast $\arg(\text{PNC}) \in (-\pi/3, \pi/3)$, $(\pi/3, \pi)$, or $(\pi, 4\pi/3)$, and then take the average within each class. In the panel insets parametrized by $x(\lambda)$ and $y(\lambda)$, we show the real space density extracted from the Bloch functions at the $M$ points, which shows a bond order that breaks the lattice rotation symmetry in real space. (b) The statistical occurrence of the nematic contrast. The nematic contrast extracted from the experimental data shows the spontaneous breaking of the three-fold lattice rotation symmetry, i.e., the emergence of the Potts-nematic order in this quantum many-body system.

Then, we divide the experimental TOF images into three classes according to their PNC values and, then, take the average within each class. The post-classification averaged results are shown in Fig. 2(a). It is evident that atoms spontaneously accumulate the $M$ points and develop phase coherence in the excited band. The kinetic energy decrease in the lattice is expected to be absorbed by the continuous degrees of freedom along the tube. From these results, the Bragg-peaks of the momentum distribution form a reciprocal lattice of the hexagonal lattice, which means the lattice translation symmetry remains unbroken. Thus, we

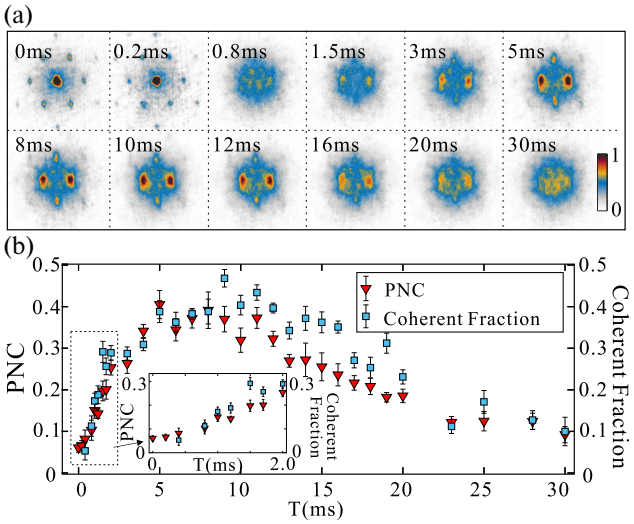


FIG. 3. Dynamical emergence of the Potts-nematic order. (a) Time evolution of momentum distribution. In (a), we average over the experimental results having a Potts-nematic contrast with $\arg(\mathrm{PNC}) \in (-\pi/3, \pi/3)$. (b) Evolution of the PNC and the coherent fraction [17]. The time point with which we quench the lattice (see Fig. 1) is set to be 0 in this plot. The phase coherence in the second band does not immediately form after the quench but, instead, appears about several milliseconds later. The emergence of the Potts-nematic order coincides with the second band phase coherence. The rise and disappearance of the Potts-nematic order define three qualitatively distinct regimes in the quantum dynamics. Here, we average over ten experimental images at each time point, with the error bar denoting the statistical error.

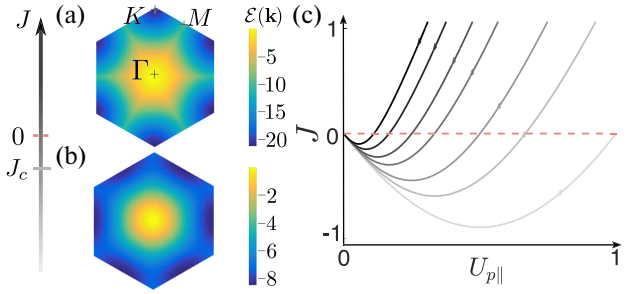


FIG. 4. Theoretical quantum phase transitions varying the orbital Josephson coupling. The orbital Josephson coupling $J$ is introduced in Eq. (2). (a) The Gross-Pitaevskii energy $\mathcal{E}(\mathbf{k})$ for a plane-wave condensate at a lattice momentum $\mathbf{k}$. Here, we choose $t_{sp}$ as an energy unit. The chemical potentials are set at $\mu_s/t_{sp} = 0.1$, $\mu_p = 0$, the interaction strengths are $U_s/t_{sp} = U_{p,\parallel}/t_{sp} = 0.5$, $J/t_{sp} = 0.4$, and $-0.4$ in (a) and (b), respectively, and $U_{p,\perp}$ is fixed respecting the lattice rotation symmetry. The energy $\mathcal{E}(\mathbf{k})$ has minima at $K$ ($M$) points for $J > J_c$ ($J < J_c$). The ground state condensates are chiral and Potts nematic, correspondingly. (c) The sketch of the renormalization of the $p$-orbital couplings to low energy. The multiple curves correspond to different choice of bare couplings. The feature of $J$ renormalizing to the negative side is generic for the hexagonal lattice. In (c), the couplings are in arbitrary units.

conclude that the observed quantum state has a Potts-nematic order. The coherent Bragg peaks suggest the system has superfluidity [41].

Since the observed Potts nematicity occurs in the excited band, it has finite lifetime and eventually decays in the dynamical evolution. In Fig. 3, we show the rise and disappearance of the Potts-nematic order in the quantum dynamics. The observation implies three different stages of dynamical evolution. At the first stage, right after atoms are loaded to the excited band, the effective mass is negative at the $\Gamma$ point causing strong dynamical instability [15], which immediately (within 1 ms) destroys the phase coherence in the lattice directions. Around 1 ms, the momentum distribution of the atoms has no sharp features [see Fig. 3(a)]. At a second stage, the atomic phase coherence starts to rebuild in the excited band around several milliseconds after getting excited, and the Potts-nematic order emerges simultaneously. The coherent Potts-nematic quantum state remains stable up to about 20 ms. The intermediate-time nematic order defines three distinctive regimes in quantum dynamics separated by the occurrence and disappearance of the spontaneous rotation symmetry breaking. Similar transient dynamics has also been found in the bipartite square lattice for a chiral Bose-Einstein condensate [11]. We expect the relatively long lifetime of the transient many-body state compared to the band relaxation time to be captured by a quantum Boltzmann equation [42].

To gain insight into the mechanism supporting the Potts-nematic order in the $sp^2$-orbital hybridized band, we provide a mean field theory analysis assuming a plane-wave condensate. Taking a trial condensate wave function with $\langle s_{\mathbf{r}} \rangle = \phi_s e^{i\mathbf{k}\cdot\mathbf{r}}$, $\langle p_{x,y,\mathbf{r}} \rangle = \phi_{x,y} e^{i\mathbf{k}\cdot\mathbf{r}}$, with $\phi_s$, $\phi_{x,y}$ the variational parameters. For each lattice momentum $\mathbf{k}$, we minimize the energy by varying $\phi_{s,x,y}$, and the resultant energy is denoted as $\mathcal{E}(\mathbf{k})$ and shown in Fig. 4. With the orbital Josephson coupling $J > 0$ [Eq. (2)], both the kinetic and interaction energies favor a condensate at $K$ points which breaks the time-reversal symmetry but respects the rotation symmetry. The corresponding condensate has a $p_x + ip_y$ character as in the square lattice [8,11]. With the Josephson coupling $J < 0$, minimizing the kinetic and the interaction energies meet frustration, as interaction then favors $p$-orbital polarization. Once the Josephson coupling is beyond a certain threshold $J < J_c \sim (-t_{sp}) < 0$, the competition between kinetic and interaction energies leads to a condensate at $M$ points, breaking the lattice rotation symmetry. Here, it is worth noting that, at the field theory tree level [43], $J$ is always positive for repulsive atoms. Thus, the observation of the Potts-nematic order in the experiment is beyond the simple mean field theory and requires considering renormalization effects. Integrating out higher momentum modes, the interaction strengths among the low-energy modes renormalize as $\Delta U_s \propto -[U_s(\Lambda)]^2$, $\Delta[U_{p\parallel} + 2J] \propto -[U_{p\parallel}(\Lambda) + 2J(\Lambda)]^2$,

$\Delta U_{p\perp} \propto -[U_{p\perp}(\Lambda)]^2$ [17]. We find that the coupling $J$ generically renormalizes to the negative side in our system due to the single-particle orbital mixing unavoidable in the hexagonal lattice (Fig. 4)—the mediated single-particle mixing between $p_x$ and $p_y$ on nearby $\mathcal{A}$ sites induced by an $s$ orbital is at the order $\hbar \times 100$ Hz according to a perturbative estimate, $t_{sp}^2/(\mu_s - \mu_p)$. The essential difference between the renormalization of $U_\perp$ and $U_\parallel$ is that it is diagonal for $U_\perp$ whereas it is nondiagonal for $U_\parallel$. The renormalization effects then stabilize the Potts-nematic order. This is in sharp contrast to the chiral $p$-orbital condensate in the square lattice [11,30], where the physics is captured within a simple mean field theory in absence of $p_x$-$p_y$ orbital mixing. The many-body renormalization effect caused phase transition has also been found for atoms in a multimode cavity [44]. Here, we remark that, although to fully determine whether the observed state is a condensate requires further interference measurements, our theory captures the Potts-nematic symmetry breaking regardless of the condensation, with thermal fluctuations taken into account [45].

*Conclusion and Outlook.*—By loading bosonic atoms into a hexagonal $sp^2$ optical lattice, we find emergence of a Potts-nematic quantum state in dynamics. The Potts-nematic order spontaneously breaks a three-fold rotation symmetry of the lattice. Our field theory analysis shows that the Potts-nematic order is stabilized by intricate renormalization effects caused by interorbital mixing. We expect our experiment to stimulate investigation of other scenarios for the Potts-nematic order as well, such as thermal fluctuations, dissipative dynamics, and lattice imperfections.

This work is supported by the National Program on Key Basic Research Project of China (Grants No. 2016YFA0301501 and No. 2017YFA0304204), the National Natural Science Foundation of China (Grants No. 61727819, No. 11934002, No. 91736208, No. 11774067, and No. 11920101004), the Natural Science Foundation of Shanghai City (Grant No. 19ZR1471500), and the Shanghai Municipal Science and Technology Major Project (Grant No. 2019SHZDZX01).

*xjzhou@pku.edu.cn
†xiaopeng_li@fudan.edu.cn

[1] P. M. Chaikin and T. C. Lubensky, *Principles of Condensed Matter Physics*, Vol. 1 (Cambridge University Press, Cambridge, England, 2000).
[2] E. Fradkin, S. A. Kivelson, M. J. Lawler, J. P. Eisenstein, and A. P. Mackenzie, Nematic fermi fluids in condensed matter physics, Annu. Rev. Condens. Matter Phys. **1**, 153 (2010).
[3] J.-H. Chu, J. G. Analytis, K. De Greve, P. L. McMahon, Z. Islam, Y. Yamamoto, and I. R. Fisher, In-plane resistivity anisotropy in an underdoped iron arsenide superconductor, Science **329**, 824 (2010).
[4] R. M. Fernandes, A. V. Chubukov, and J. Schmalian, What drives nematic order in iron-based superconductors?, Nat. Phys. **10**, 97 (2014).
[5] Q. Si, R. Yu, and E. Abrahams, High-temperature superconductivity in iron pnictides and chalcogenides, Nat. Rev. Mater. **1**, 16017 (2016).
[6] R. M. Fernandes, P. P. Orth, and J. Schmalian, Intertwined vestigial order in quantum materials: Nematicity and beyond, Annu. Rev. Condens. Matter Phys. **10**, 133 (2019).
[7] M. Lewenstein and W. V. Liu, Optical lattices: Orbital dance, Nat. Phys. **7**, 101 (2011).
[8] X. Li and W. V. Liu, Physics of higher orbital bands in optical lattices: A review, Rep. Prog. Phys. **79**, 116401 (2016).
[9] C. V. Parker, L.-C. Ha, and C. Chin, Direct observation of effective ferromagnetic domains of cold atoms in a shaken optical lattice, Nat. Phys. **9**, 769 (2013).
[10] L. Niu, S. Jin, X. Chen, X. Li, and X. Zhou, Observation of a Dynamical Sliding Phase Superfluid with $p$-Band Bosons, Phys. Rev. Lett. **121**, 265301 (2018).
[11] G. Wirth, M. Ölschläger, and A. Hemmerich, Evidence for orbital superfluidity in the $P$-band of a bipartite optical square lattice, Nat. Phys. **7**, 147 (2011).
[12] T. Kock, M. Olschlager, A. Ewerbeck, W. M. Huang, L. Mathey, and A. Hemmerich, Observing Chiral Superfluid Order by Matter-Wave Interference, Phys. Rev. Lett. **114**, 115301 (2015).
[13] J. Struck, C. Olschlager, R. Le Targat, P. Soltan-Panahi, A. Eckardt, M. Lewenstein, P. Windpassinger, and K. Sengstock, Quantum simulation of frustrated classical magnetism in triangular optical lattices, Science **333**, 996 (2011).
[14] P. Soltan-Panahi, D.-S. Lühmann, J. Struck, P. Windpassinger, and K. Sengstock, Quantum phase transition to unconventional multi-orbital superfluidity in optical lattices, Nat. Phys. **8**, 71 (2012).
[15] C. J. Pethick and H. Smith, *Bose–Einstein Condensation in Dilute Gases* (Cambridge University Press, Cambridge, England, 2008).
[16] D. M. Stamper-Kurn and M. Ueda, Spinor Bose gases: Symmetries, magnetism, and quantum dynamics, Rev. Mod. Phys. **85**, 1191 (2013).
[17] See Supplemental Material at http://link.aps.org/supplemental/10.1103/PhysRevLett.126.035301 for detailed theoretical analysis of the observed Potts-nematic quantum state, and additional information on experimental protocols and data analysis, which includes Refs. [18–26].
[18] S. Jin, X. Guo, P. Peng, X. Chen, X. Li, and X. Zhou, Finite temperature phase transition in a cross-dimensional triangular lattice, New J. Phys. **21**, 073015 (2019).
[19] Y. B. Ovchinnikov, J. H. Muller, M. R. Doery, E. J. D. Vredenbregt, K. Helmerson, S. L. Rolston, and W. D. Phillips, Diffraction of a Released Bose-Einstein Condensate by a Pulsed Standing Light Wave, Phys. Rev. Lett. **83**, 284 (1999).
[20] B. Gadway, D. Pertot, R. Reimann, M. G. Cohen, and D. Schneble, Analysis of Kapitza-Dirac diffraction patterns beyond the Raman-Nath regime, Opt. Express **17**, 19173 (2009).

[21] T. Zhou, K. Yang, Y. Zhai, X. Yue, S. Yang, J. Xiang, Q. Huang, W. Xiong, X. Zhou, and X. Chen, High precision calibration of optical lattice depth based on multiple pulses Kapitza-Dirac diffraction, Opt. Express **26**, 16726 (2018).
[22] C. Schori, T. Stöferle, H. Moritz, M. Köhl, and T. Esslinger, Excitations of a Superfluid in a Three-Dimensional Optical Lattice, Phys. Rev. Lett. **93**, 240402 (2004).
[23] K. Günter, T. Stöferle, H. Moritz, M. Köhl, and T. Esslinger, Bose-Fermi Mixtures in a Three-Dimensional Optical Lattice, Phys. Rev. Lett. **96**, 180402 (2006).
[24] C. K. Thomas, T. H. Barter, T. H. Leung, M. Okano, G. B. Jo, J. Guzman, I. Kimchi, A. Vishwanath, and D. M. Stamper-Kurn, Mean-Field Scaling of the Superfluid to Mott Insulator Transition in a 2D Optical Superlattice, Phys. Rev. Lett. **119**, 100402 (2017).
[25] D. Jaksch, C. Bruder, J. I. Cirac, C. W. Gardiner, and P. Zoller, Cold Bosonic Atoms in Optical Lattices, Phys. Rev. Lett. **81**, 3108 (1998).
[26] S. Raghu and S. A. Kivelson, Superconductivity from repulsive interactions in the two-dimensional electron gas, Phys. Rev. B **83**, 094518 (2011).
[27] K. Sun, W. V. Liu, A. Hemmerich, and S. D. Sarma, Topological semimetal in a fermionic optical lattice, Nat. Phys. **8**, 67 (2012).
[28] X. Li, E. Zhao, and W. V. Liu, Topological states in a ladder-like optical lattice containing ultracold atoms in higher orbital bands, Nat. Commun. **4**, 1523 (2013).
[29] B. Liu, X. Li, B. Wu, and W. V. Liu, Chiral superfluidity with $p$-wave symmetry from an interacting $s$-wave atomic fermi gas, Nat. Commun. **5**, 5064 (2014).
[30] B. Liu, X.-L. Yu, and W.-M. Liu, Renormalization-group analysis of $p$-orbital Bose-Einstein condensates in a square optical lattice, Phys. Rev. A **88**, 063605 (2013).
[31] C. Wu, W. V. Liu, J. Moore, and S. D. Sarma, Quantum Stripe Ordering in Optical Lattices, Phys. Rev. Lett. **97**, 190406 (2006).
[32] C. Wu, Orbital Ordering and Frustration of $p$-Band Mott Insulators, Phys. Rev. Lett. **100**, 200406 (2008).
[33] E. Zhao and W. V. Liu, Orbital Order in Mott Insulators of Spinless $p$-Band Fermions, Phys. Rev. Lett. **100**, 160403 (2008).
[34] Z.-F. Xu, L. You, A. Hemmerich, and W. V. Liu, $\pi$-Flux Dirac Bosons and Topological Edge Excitations in a Bosonic Chiral $p$-Wave Superfluid, Phys. Rev. Lett. **117**, 085301 (2016).
[35] G. Grynberg, B. Lounis, P. Verkerk, J.-Y. Courtois, and C. Salomon, Quantized Motion of Cold Cesium Atoms in Two- and Three-Dimensional Optical Potentials, Phys. Rev. Lett. **70**, 2249 (1993).
[36] C. Becker, P Soltan-Panahi, J. Kronjäger, S. Dörscher, K. Bongs, and K. Sengstock, Ultracold quantum gases in triangular optical lattices, New J. Phys. **12**, 065025 (2010).
[37] P. Soltan-Panahi, J. Struck, P. Hauke, A. Bick, W. Plenkers, G. Meineke, C. Becker, P. Windpassinger, M. Lewenstein, and K. Sengstock, Multi-component quantum gases in spin-dependent hexagonal lattices, Nat. Phys. **7**, 434 (2011).
[38] Y. Xia *et al.*, Observation of a large-gap topological-insulator class with a single dirac cone on the surface, Nat. Phys. **5**, 398 (2009).
[39] G.-F. Zhang, Y. Li, and C. Wu, Honeycomb lattice with multiorbital structure: Topological and quantum anomalous hall insulators with large gaps, Phys. Rev. B **90**, 075114 (2014).
[40] V. Meunier, A. G. Souza Filho, E. B. Barros, and M. S. Dresselhaus, Physical properties of low-dimensional $sp^2$-based carbon nanostructures, Rev. Mod. Phys. **88**, 025005 (2016).
[41] M. Greiner, O. Mandel, T. Esslinger, T. W. Hänsch, and I. Bloch, Quantum phase transition from a superfluid to a Mott insulator in a gas of ultracold atoms, Nature (London) **415**, 39 (2002).
[42] V. Sharma, S. Choudhury, and E. J. Mueller, Dynamics of Bose-Einstein recondensation in higher bands, Phys. Rev. A **101**, 033609 (2020).
[43] R. Shankar, Renormalization-group approach to interacting fermions, Rev. Mod. Phys. **66**, 129 (1994).
[44] S. Gopalakrishnan, Y. E. Shchadilova, and E. Demler, Intertwined and vestigial order with ultracold atoms in multiple cavity modes, Phys. Rev. A **96**, 063828 (2017).
[45] X. Li, A. Paramekanti, A. Hemmerich, and W. V. Liu, Proposed formation and dynamical signature of a chiral Bose liquid in an optical lattice, Nat. Commun. **5**, 3205 (2014).